

Self-Supervised Poisson-Gaussian Denoising

Wesley Khademi¹, Sonia Rao², Clare Minnerath³, Guy Hagen⁴, and Jonathan Ventura¹

¹California Polytechnic State University

²University of Georgia

³Providence College

⁴University of Colorado Colorado Springs

Abstract

We extend the blindspot model for self-supervised denoising to handle Poisson-Gaussian noise and introduce an improved training scheme that avoids hyperparameters and adapts the denoiser to the test data. Self-supervised models for denoising learn to denoise from only noisy data and do not require corresponding clean images, which are difficult or impossible to acquire in some application areas of interest such as low-light microscopy. We introduce a new training strategy to handle Poisson-Gaussian noise which is the standard noise model for microscope images. Our new strategy eliminates hyperparameters from the loss function, which is important in a self-supervised regime where no ground truth data is available to guide hyperparameter tuning. We show how our denoiser can be adapted to the test data to improve performance. Our evaluation on a microscope image denoising benchmark validates our approach.

1 Introduction

Fluorescence microscopy is a vital tool for understanding cellular processes and structures. Because fluorescence imaging with long exposure times or intense illumination may damage the cell sample through phototoxicity, fluorescence microscopy images are typically acquired under photon-limited conditions. However, safely imaging the cell using low light conditions and/or low exposure times unfortunately lowers the signal-to-noise ratio (SNR), hindering further analysis and interpretation of the resulting images.

The SNR is the product of a combination of factors, including exposure time, excitation intensity, and camera characteristics. In fluorescence microscopy, the noise is typically described by a Poisson-Gaussian model (Foi et al., 2008). The goal of image denoising is to computationally increase the image SNR (Figure 1). In contrast to traditional methods (Chambolle, 2004; Dabov et al., 2006; Blu and Luisier, 2007; Luisier et al., 2010; Buades et al., 2011; Gu et al., 2014) which denoise based on only the input image, learning-based methods learn to denoise from a dataset of example images.

In recent years, deep learning methods using convolutional neural networks have shown significant promise in learning-based fluorescence microscopy image denoising (Zhang et al., 2017; Weigert et al., 2018). However, the supervised approach to learning denoising faces practical limitations because it requires a large number of corresponding pairs of low SNR and high SNR images. When imaging live cells, for example, it is not possible to acquire paired low and high SNR images for training because a) the sample is moving and b) exposure to light causes photobleaching and ultimately kills the sample.

For these reasons, researchers have turned to self-supervised approaches to denoising (Soltanayev and Chun, 2018; Batson and Royer, 2019; Krull et al., 2019a; Laine et al., 2019). In the self-supervised setting, the learner only has access to low SNR images. Of the recent approaches, blindspot neural networks (Laine et al., 2019) have shown the best performance. In this work, we address two shortcomings of blindspot neural networks for self-supervised denoising:

1. We introduce a loss function appropriate for Poisson-Gaussian noise which is the standard model for microscope images;
2. We introduce an alternate training strategy which eliminates the need to regularize the loss function; this is critical in the self-supervised setting where no ground truth validation data is available to tune the regularization strength.

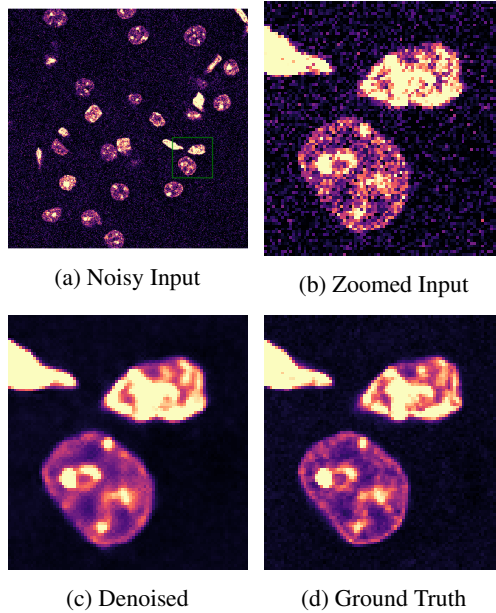


Figure 1: An example of our self-supervised denoising result. Image from the Confocal Mice dataset (Zhang et al., 2019).

In the following, we survey related work on self-supervised denoising (Section 2), review the blindspot neural network approach to self-supervised denoising (Section 3), introduce our new uncalibrated approach (Section 4), present the results of our evaluation and comparison to competing methods on benchmark datasets (Section 5), and provide conclusions and directions for future work (Section 6).

2 Related Work

2.1 Traditional methods

Many traditional methods for denoising such as BM3D (Dabov et al., 2006), non-local means (Buades et al., 2011), and weighted non-nuclear norm minimization (Gu et al., 2014) perform denoising by comparing the neighborhood of a pixel to other similar regions in the image. The advantage of learning-based methods is that they can also take advantage of examples from other images in the dataset beyond the input image to be denoised. Other methods such as total-variation denoising (Chambolle, 2004) enforce smoothness priors on the image which tend to lead to highly quantized results.

While most previous methods for denoising are designed for additive Gaussian noise; in the case of Poisson-Gaussian noise, a variance stabilizing transform (Makitalo and Foi, 2012) is applied to approximately transform the noise to be Gaussian. However, these methods are designed explicitly for Poisson-Gaussian noise (Luisier et al., 2010).

2.2 Deep learning methods

At present, supervised deep learning methods for denoising (Zhang et al., 2017; Weigert et al., 2018) typically far outperform traditional and self-supervised methods in terms of peak signal-to-noise ratio (PSNR). Most supervised methods apply a fully convolutional neural network (Long et al., 2015; Ronneberger et al., 2015) and simply regress to the clean image.

Recently, several approaches to self-supervised denoising have been developed. Some methods (Soltanayev and Chun, 2018) use as a loss function Stein’s Unbiased Risk Estimate (SURE) (Stein, 1981; Ramani et al., 2008), which estimates the mean squared error (MSE) between a denoised image and the clean image without actually having access to the clean image. An analogous estimator for Poisson-Gaussian noise has been developed (Luisier et al., 2010). However, these methods require *a priori* knowledge of the noise level which is unrealistic in a practical setting. Our approach supports blind denoising and adaptively estimates the noise level at test time.

Lehtinen et al. (2018) introduced a highly successful approach to self-supervised denoising called Noise2Noise. In this approach, the network learns to transform one noisy instantiation of a clean image into another; under the MSE loss function, the network learns to output the expected value of the data which corresponds to the clean image. While this method can achieve results very close to a supervised method, it requires multiple, corresponding noisy images and thus is similarly limited in application in the live cell microscopy context.

An alternate approach to self-supervised denoising which does not require multiple noise instantiations of the same clean image is to learn a filter which predicts the center pixel of the receptive field based on the surrounding neighborhood of noisy pixels. By training such a filter to minimize the MSE to the noisy input, the resulting filter will theoretically output the clean value (Batson and Royer, 2019; Krull et al., 2019a). Laine et al. (2019) refer to a neural network built around this concept as a “blindspot neural network.” They improved upon the blindspot concept by extending it to a Bayesian context and introduced loss functions for pure Gaussian or Poisson noise, showing results very close to the supervised result when trained on synthetically noised data. However, their method requires a regularization term in the loss function which can’t practically be tuned in the self-supervised setting; in our evaluation we found that the regularization strength indeed needs to be tuned for best results on different datasets. Our method avoids the need for regularization and outperforms the regularized version in our experiments.

Krull et al. (2019b) introduced Probabilistic Noise2Void (PN2V) which takes a non-parametric approach to modeling both the noise distribution and the network output; however, their approach requires paired clean and noisy images in order to calibrate the noise model. A recent follow-on work called PPN2V (Prakash et al., 2020) estimates the noise model using a Gaussian Mixture Model (GMM) in a fully unsupervised manner. Again, this approach involves several hyperparameters controlling the complexity of the noise model which need to be tuned, while ours does not. Additionally, in our experiments, we show that our approach outperforms PPN2V on several datasets.

3 Self-supervised learning of denoising

The goal of denoising is to predict the values of a “clean” image $\mathbf{x} = (x_1, \dots, x_n)$ given a “noisy” image $\mathbf{y} = (y_1, \dots, y_n)$. We make the common assumption that each clean pixel x_i depends on the noisy pixels in a neighborhood Ω_{y_i} around that pixel. We also assume that the noise at each pixel is sampled independently.

Following Laine et al. (2019) and Krull et al. (2019b), we can connect y_i to its neighborhood Ω_{y_i} by marginalizing out the unknown clean value x_i :

$$\underbrace{p(y_i|\Omega_{y_i})}_{\text{Noisy observation}} = \int \underbrace{p(y_i|x_i)}_{\text{Noise model}} \underbrace{p(x_i|\Omega_{y_i})}_{\text{Clean prior}} dx_i. \quad (1)$$

Since we only have access to observations of y_i for training, this formulation allows us to fit a model for the clean data by minimizing the negative log likelihood of the noisy data, i.e. minimizing a loss function defined as

$$\mathcal{L}^{\text{marginal}} = \sum_i -\log p(y_i|\Omega_{y_i}). \quad (2)$$

In the following we will drop the Ω_{y_i} to save space.

3.1 Poisson-Gaussian noise

In the case of Poisson-Gaussian noise, the noisy observation y_i is sampled by first applying Poisson corruption to x_i and then adding Gaussian noise which is independent of x_i . We have

$$y_i = aP(x_i/a) + N(0, b) \quad (3)$$

where $a > 0$ is a scaling factor (related to the gain of the camera) and b is the variance of the Gaussian noise component, which models other sources of noise such as electric and thermal noise (Foi et al., 2008).

We apply the common approximation of the Poisson distribution as a Gaussian with equal mean and variance:

$$y_i \approx aN(x_i/a, x_i/a) + N(0, b) \quad (4)$$

$$= N(x_i, ax_i + b). \quad (5)$$

The noise model is then simply a Gaussian noise model whose variance is an affine transformation of the clean value. Note that in practice we allow b to be negative; this models the effect of an offset or “pedestal” value in the imaging system (Foi et al., 2008). This general formulation encompasses both pure Gaussian ($a = 0$) and Poisson noise ($b = 0$).

3.2 Choice of prior

In order to implement our loss function (Equation 2) we need to choose a form for the prior $p(x_i|\Omega_{y_i})$ that makes the integral tractable. One approach is to use the conjugate prior of the noise model $p(y_i|x_i)$, so that the integral can be computed analytically. For example, Laine et al. (2019) model the prior $p(x_i|\Omega_{y_i})$ as a Gaussian, so that the marginal is also a Gaussian. Alternatively, Krull et al. (2019b) take a non-parametric approach and sample the prior.

In this work, similar to Laine et al. (2019) we model the prior as a Gaussian with mean μ_i and variance σ_i^2 . We replace the ax term in Equation 4 with $a\mu$ to make the integral in Equation 2 tractable; this approximation should be accurate as long as σ_i^2 is small. The marginal distribution of y_i is then

$$p(y_i) = \frac{1}{\sqrt{2\pi(a\mu_i + b + \sigma_i^2)}} \exp\left(-\frac{(y_i - \mu_i)^2}{2(a\mu_i + b + \sigma_i^2)}\right) \quad (6)$$

and the corresponding loss function is

$$\mathcal{L}^{\text{marginal}} = \sum_i \left(\frac{(y_i - \mu_i)^2}{a\mu_i + b + \sigma_i^2} + \log(a\mu_i + b + \sigma_i^2) \right) \quad (7)$$

3.3 Posterior mean estimate

At test time, μ_i is an estimate of the clean value x_i based on Ω_{y_i} , the neighborhood of noisy pixels around y_i . However, this estimate does not take into account the actual value of y_i which potentially provides useful information about x_i .

Laine et al. (2019) and Krull et al. (2019b) suggest to instead use the expected value of the posterior to maximize the PSNR of the resulting denoised image. In our case we have

$$\hat{x}_i = \mathbb{E}[p(x_i|y_i)] = \frac{y_i\sigma_i^2 + (a\mu_i + b)\mu_i}{a\mu_i + b + \sigma_i^2}. \quad (8)$$

Intuitively, when the prior uncertainty is large relative to the noise estimate, the formula approaches the noisy value y_i ; when the prior uncertainty is small relative to the noise estimate, the formula approaches the prior mean μ_i .

3.4 Blindspot neural network

In our approach, μ_i and σ_i^2 are the outputs of a blindspot neural network (Laine et al., 2019) and a and b are global parameters learned along with the network parameters.

The “blind-spot neural network” is constructed in such a way that the network cannot see input y_i when outputting the parameters for $p(x_i)$. The blindspot effect can be achieved in multiple ways. Noise2Void (Krull et al., 2019a) and Noise2Self (Batson and Royer, 2019) replace a random subset of pixels in each batch and mask out those pixels in the loss computation. Laine et al. (2019) instead construct a fully convolutional neural network in such a way that the center of the receptive field is hidden from the neural network input. In our experiments we use the same blindspot neural network architecture as Laine et al. (2019).

3.5 Regularization

In a practical setting, the parameters a and b of the noise model are not known *a priori*; instead, we need to estimate them from the data. However, an important issue arises when attempting to learn the noise parameters along with the network parameters: the network’s prior uncertainty and noise estimate are essentially interchangeable without any effect on the loss function. In other words, the optimizer is free to increase a and b and decrease σ_i^2 , or vice-versa, without any penalty. To combat this, we add a regularization term to the per-pixel loss which encourages the prior uncertainty to be small:

$$\mathcal{L}^{\text{regularized}} = \mathcal{L}^{\text{marginal}} + \lambda \sum_i |\sigma_i|. \quad (9)$$

We found in our experiments that the choice of λ strongly affects the results. When λ is too high, the prior uncertainty is too small, and the results are blurry. When λ is too low, the prior uncertainty is too high, and the network does not denoise at all. Unfortunately, in the self-supervised setting, it is not possible to determine the appropriate setting of λ using a validation set, because we do not have ground truth “clean” images with which to evaluate a particular setting of λ .

4 Learning an uncalibrated model

This realization led us to adopt a different training strategy which defers the learning of the noise parameter models to test time.

In our uncalibrated model, we do not separate out the parameters of the noise model from the parameters of the prior. Instead, we learn a single variance value $\hat{\sigma}_i^2$ representing the total uncertainty of the network. Our uncalibrated loss function is then

$$\mathcal{L}^{\text{uncalibrated}} = \sum_i \left(\frac{(y_i - \mu_i)^2}{\hat{\sigma}_i^2} + \log(\hat{\sigma}_i^2) \right) \quad (10)$$

At test time, however, we need to know the noise parameters a and b in order to compute $\sigma_i^2 = \hat{\sigma}_i^2 - a\mu_i - b$ and ultimately compute our posterior mean estimate \hat{x}_i .

If we had access to corresponding clean and noisy observations (x_i and y_i , respectively) then we could fit a Poisson-Gaussian noise model to the data in order to learn a and b . In other words, we would find

$$a, b = \arg \min_{a, b} \sum_i \left(\frac{(y_i - x_i)^2}{ax_i + b} + \log(ax_i + b) \right). \quad (11)$$

As we are in a self-supervised setting, however, we do not have access to clean data. Instead, we propose to use the prior mean μ_i as a stand-in for the actual clean value x_i . This bootstrapping approach is similar to that proposed by Prakash et al. (2020); however, they fit a general parametric noise model to the training data where as we propose to fit a Poisson-Gaussian model to each image in the test set.

Our approach is summarized in the following steps:

1. Train a blindspot neural network to model the noisy data by outputting a mean and variance value at each pixel, using the uncalibrated loss function (Equation 10).
2. For each test image:
 - i. Run the blindspot neural network with the noisy image as input to obtain mean μ_i and total variance $\hat{\sigma}_i^2$ estimate at each pixel.
 - ii. Determine the optimal noise parameters a, b by fitting a Poisson-Gaussian distribution to the noisy and psuedo-clean images given by the mean values of the network output (Equation 30).
 - iii. Calculate the prior uncertainty at each pixel as $\sigma_i^2 = \max(0.0001, \hat{\sigma}_i^2 - a\mu_i - b)$.
 - iv. Use the noise parameters a, b and the calculated prior uncertainties σ_i^2 to compute the denoised image as the posterior mean estimate (Equation 8).

5 Experiments and Results

5.1 Implementation details

Our implementation uses the Keras library with Tensorflow backend. We use the same blindspot neural network architecture as Laine et al. (2019). We use the Adam optimizer (Kingma and Ba, 2014) with a learning rate of 0.0003 over 300 epochs, halving the learning rate when the validation loss plateaued. Each epoch consists of 50 batches of 128×128 crops from random images from the training set. For data augmentation we apply random rotation (in multiples of 90 degrees) and horizontal/vertical flipping.

To fit the Poisson-Gaussian noise parameters at test time, we apply Nelder-Mead optimization (Nelder and Mead, 1965) with $(a = 0.01, b = 0)$ as the initialization point. We cut off data in the bottom 2% and top 3% of the noisy image’s dynamic range before estimating the noise parameters.

5.2 Datasets

We evaluated our method on two datasets consisting of real microscope images captured with various imaging setups and types of samples. Testing on real data gives us a more accurate evaluation of our method’s performance in contrast to training and testing on synthetically noised data, since real data is not guaranteed to follow the theoretical noise model.

The fluorescence microscopy denoising (FMD) benchmark (Zhang et al., 2019) contains a total of 12 datasets of images captured using either a confocal, two-photon, or widefield microscope. We used the same subset of datasets (Confocal Mice, Confocal Fish, and Two-Photon Mice) used to evaluate PN2V (Krull et al., 2019b) so that we could compare our results. Each dataset consists of 20 views of the sample with 50 noisy images per view. The 19th-view is withheld for testing, and the ground truth images are created by averaging the noisy images in each view. We trained a denoising model on the raw noisy images in each dataset separately.

Prakash et al. (2020) evaluated PPN2V on three sequences from a confocal microscope, imaging *Convallaria*, Mouse Nuclei, and Mouse Actin. Each sequence consists of 100 noisy images and again the clean image is computed as the average of the noisy images. Whereas the FMD dataset provides 8-bit images clipped at 255, these images are 16-bit and thus are not clipped. Following their evaluation procedure, each method is trained on all 100 images and then tested on a crop of the same 100 images; this methodology is allowable in the self-supervised context since no label data is used during training.

5.3 Experiments

In the following we will refer to the competing methods under consideration as

- **Regularized (Ours):** Blindspot neural network trained using the regularized Poisson-Gaussian loss function (Equation 2) with regularization strength λ .
- **Uncalibrated (Ours):** Blindspot neural network trained using the uncalibrated loss function (Equation 10) with noise parameter estimation done adaptively at test time (Section 4).
- **N2V:** Noise2Void which uses the MSE loss function and random masking to create the blindspot effect (Krull et al., 2019a).
- **PN2V:** Probabilistic Noise2Void – same setup as N2V but uses a histogram noise model created from the ground truth data and a non-parametric prior (Krull et al., 2019b).
- **Bootstrap GMM and Bootstrap Histogram:** PPN2V training – same setup as PN2V but models the noise distribution using either a GMM or histogram fit to the Noise2Void output (Prakash et al., 2020).
- **U-Net:** U-Net (Ronneberger et al., 2015) trained for denoising in a supervised manner using MSE loss (Weigert et al., 2018).
- **N2N:** Noise2Noise training using MSE loss (Lehtinen et al., 2018).

5.3.1 Noise parameter estimation

We first evaluate whether our bootstrap approach to estimating the Poisson-Gaussian noise parameters is accurate in comparison to estimating the noise parameters using the actual ground truth clean values.

Figure 2 shows a comparison of the bootstrap and ground truth noise models using an image from the Two-Photon Mice dataset. There is little difference between the bootstrap and ground truth pdfs and both models appear to fit the true data distribution well.

5.3.2 Effect of regularization

To highlight the difficulties of hyperparameter tuning in the self-supervised context, we trained our uncalibrated model and several regularized models on the FMD datasets. We tested a regularization strength of $\lambda = 0.1, 1, \text{ and } 10$.

The results are shown in Table 1. The test set PSNR of the regularized model varies greatly depending on the setting of λ , and indeed a different setting of λ is optimal for each dataset. This indicates that hyperparameter tuning is critical for the regularized approach, but it is not actually possible in a self-supervised context.

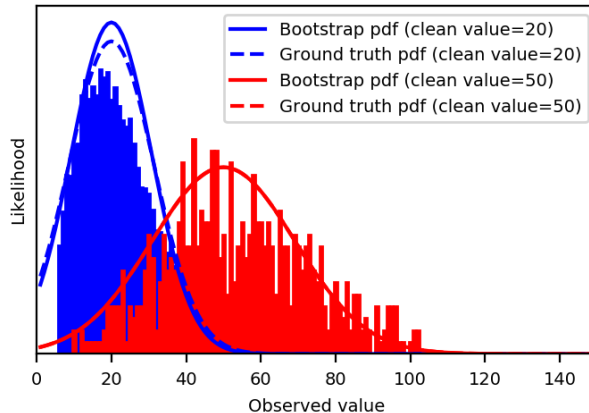


Figure 2: Comparison of Poisson-Gaussian noise models fit to a noisy image from the Two-Photon Mice dataset. The solid bars show histograms of the noisy values corresponding to a clean value of 20 (blue) and 50 (red). The curves show the pdfs of a Poisson-Gaussian distribution fit to the data using either the ground truth clean data (dashed line) or the initial denoised estimate from the prior (solid line). Here the ground truth estimate was ($a = 0.3061226, b = -0.00040798$) and the bootstrap estimate was ($a = 0.03245783, b = -0.00077324$).

Methods	λ	Confocal Mice	Confocal Zebrafish	Two-Photon Mice
Uncalibrated	-	37.97	32.26	33.83
Regularized	0.1	37.74	23.97	33.52
Regularized	1	37.64	27.44	33.56
Regularized	10	37.13	31.99	33.34

Table 1: Comparison between uncalibrated and regularized methods. The uncalibrated method outperforms the regularized method at any setting of λ .

In contrast, our uncalibrated method outperforms the regularized method at any setting of λ , and does not require any hyperparameters.

5.3.3 Comparison to state-of-the-art

Next we present the results of our performance evaluation on the FMD and PPN2V benchmark datasets. Table 2 shows a comparison between our uncalibrated method and various competing methods, including self-supervised and supervised methods.

Between the fully unsupervised methods that do not require paired noisy images (our Uncalibrated method, N2V, Bootstrap GMM, and Bootstrap Histogram), our method outperforms the others on four out of six datasets. An example result from our method is shown in Figure 3 and a comparison of denoising results are shown in Figure 4.

6 Conclusions and Future Work

Noise is an unavoidable artifact of imaging systems, and for some applications such as live cell microscopy, denoising is a critical processing step to support quantitative and qualitative analysis. In this work, we have introduced a powerful new scheme for self-supervised learning of denoising which is appropriate for processing of low-light images. In contrast to the state-of-the-art, our model handles Poisson-Gaussian noise which is the standard noise model for most imaging systems including digital microscopes. In addition, we eliminate the need for loss function regularization in our method, thus making self-supervised denoising more practically applicable. Our evaluation real datasets shows that our method outperforms competing methods in terms of the standard PSNR metric on many datasets tested.

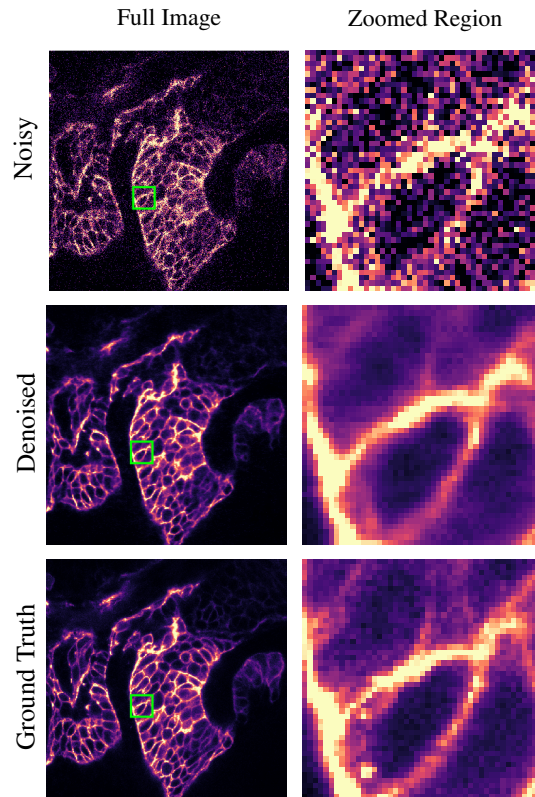


Figure 3: Example denoising result on the Confocal Fish dataset.

Our work opens up new avenues in live-cell imaging such as extreme low-light imaging over long periods of time. Future work lies in extending our model to other noise models appropriate to other imaging modalities, and exploring how to overcome the limitations of the approach for imaging modalities where the assumptions of Poisson-Gaussian noise and/or noise independence between pixels are not valid.

Acknowledgements

This work was supported in part by National Science Foundation under award number 1659788 and the National Institutes of Health under award number 1R15GM128166-01. This work was also supported by the University of Colorado Colorado Springs Biofrontiers Center.

References

- Batson, J. and Royer, L. (2019). Noise2self: Blind denoising by self-supervision. In *The 36th International Conference on Machine Learning (ICML 2019)*.
- Blu, T. and Luisier, F. (2007). The sure-let approach to image denoising. *IEEE Transactions on Image Processing*, 16(11):2778–2786.
- Buades, A., Coll, B., and Morel, J.-M. (2011). Non-local means denoising. *Image Processing On Line*, 1:208–212.
- Chambolle, A. (2004). An algorithm for total variation minimization and applications. *Journal of Mathematical imaging and vision*, 20(1-2):89–97.

Methods	Confocal Mice	Confocal Zebrafish	Two-Photon Mice	Convallaria	Mouse Nuclei	Mouse Actin
Uncalibrated (Ours)	37.97	32.26	33.83	36.44	36.97	33.35
N2V	37.56	32.10	33.42	35.73	35.84	33.39
Bootstrap GMM	37.86	*	33.77	36.70	36.43	33.74
Bootstrap Histogram	36.98	32.23	33.53	36.19	36.31	33.61
PN2V	38.24	32.45	33.67	36.51	36.29	33.78
U-Net	38.38	32.93	34.35	36.71	36.58	34.20
N2N	38.19	32.93	34.33	-	-	-

Table 2: Quantitative comparison of our implementation and baseline methods on datasets provided by Zhang et al. (2019) and Prakash et al. (2020). Methods above the solid line are fully unsupervised while those below it either require ground truth data or a noisy image pair. Bold numbers indicate the best performing method among the fully unsupervised methods. The * indicates a case where the Bootstrap GMM method failed to train (the loss became NaN before convergence).

Dabov, K., Foi, A., Katkovnik, V., and Egiazarian, K. (2006). Image denoising with block-matching and 3d filtering. In *Image Processing: Algorithms and Systems, Neural Networks, and Machine Learning*, volume 6064, page 606414. International Society for Optics and Photonics.

Foi, A., Trimeche, M., Katkovnik, V., and Egiazarian, K. (2008). Practical poissonian-gaussian noise modeling and fitting for single-image raw-data. *IEEE Transactions on Image Processing*, 17(10):1737–1754.

Gu, S., Zhang, L., Zuo, W., and Feng, X. (2014). Weighted nuclear norm minimization with application to image denoising. In *Proceedings of the IEEE conference on computer vision and pattern recognition*, pages 2862–2869.

Kingma, D. P. and Ba, J. (2014). Adam: A method for stochastic optimization. In *International Conference on Learning Representations (ICLR)*.

Krull, A., Buchholz, T.-O., and Jug, F. (2019a). Noise2void-learning denoising from single noisy images. In *Proceedings of the IEEE Conference on Computer Vision and Pattern Recognition*, pages 2129–2137.

Krull, A., Vicar, T., and Jug, F. (2019b). Probabilistic noise2void: Unsupervised content-aware denoising. *arXiv preprint arXiv:1906.00651*.

Laine, S., Karras, T., Lehtinen, J., and Aila, T. (2019). High-quality self-supervised deep image denoising. In *Advances in Neural Information Processing Systems*, pages 6968–6978.

Lehtinen, J., Munkberg, J., Hasselgren, J., Laine, S., Karras, T., Aittala, M., and Aila, T. (2018). Noise2Noise: Learning image restoration without clean data. In *International Conference on Machine Learning*.

Long, J., Shelhamer, E., and Darrell, T. (2015). Fully convolutional networks for semantic segmentation. In *Proceedings of the IEEE conference on computer vision and pattern recognition*, pages 3431–3440.

Luisier, F., Blu, T., and Unser, M. (2010). Image denoising in mixed poisson–gaussian noise. *IEEE Transactions on image processing*, 20(3):696–708.

Makitalo, M. and Foi, A. (2012). Optimal inversion of the generalized anscombe transformation for poisson-gaussian noise. *IEEE transactions on image processing*, 22(1):91–103.

Nelder, J. A. and Mead, R. (1965). A simplex method for function minimization. *The computer journal*, 7(4):308–313.

Prakash, M., Lalit, M., Tomancak, P., Krull, A., and Jug, F. (2020). Fully unsupervised probabilistic noise2void. In *International Symposium on Biomedical Imaging (ISBI 2020)*.

Ramani, S., Blu, T., and Unser, M. (2008). Monte-carlo sure: A black-box optimization of regularization parameters for general denoising algorithms. *IEEE Transactions on image processing*, 17(9):1540–1554.

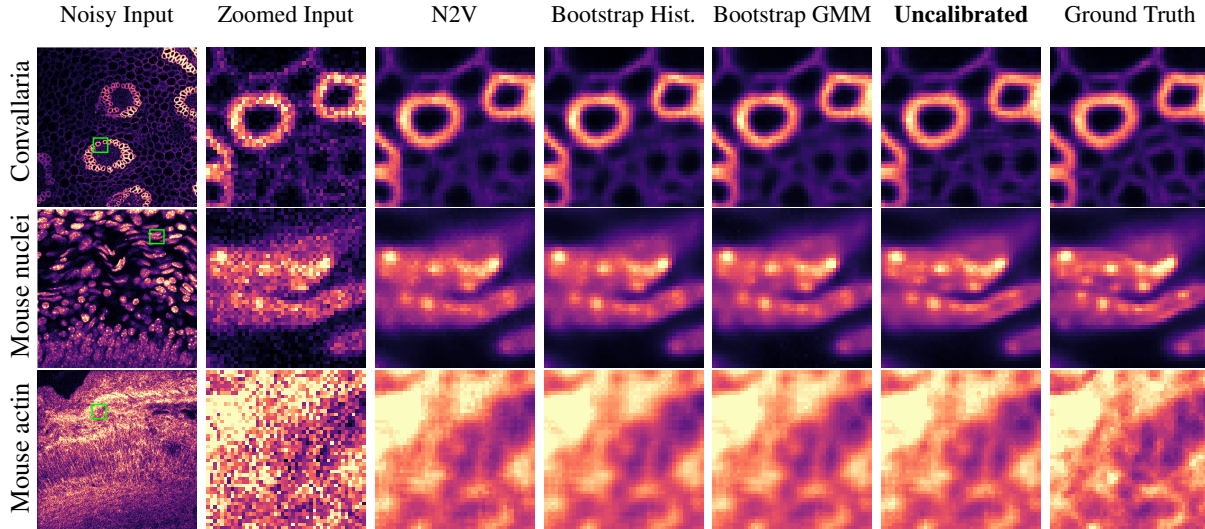


Figure 4: Visual comparison of results obtained by our proposed method and the fully unsupervised methods listed in Table 2. Noisy test images taken from PPN2V benchmark datasets (Prakash et al., 2020). Green boxes found in images in the leftmost column denote the regions zoomed in on for qualitative denoising evaluation.

Ronneberger, O., Fischer, P., and Brox, T. (2015). U-net: Convolutional networks for biomedical image segmentation. In *International Conference on Medical image computing and computer-assisted intervention*, pages 234–241. Springer.

Soltanayev, S. and Chun, S. Y. (2018). Training deep learning based denoisers without ground truth data. In *Advances in Neural Information Processing Systems*, pages 3257–3267.

Stein, C. M. (1981). Estimation of the mean of a multivariate normal distribution. *The annals of Statistics*, pages 1135–1151.

Weigert, M., Schmidt, U., Boothe, T., Müller, A., Dibrov, A., Jain, A., Wilhelm, B., Schmidt, D., Broaddus, C., Culley, S., et al. (2018). Content-aware image restoration: pushing the limits of fluorescence microscopy. *Nature methods*, 15(12):1090–1097.

Zhang, K., Zuo, W., Chen, Y., Meng, D., and Zhang, L. (2017). Beyond a gaussian denoiser: Residual learning of deep cnn for image denoising. *IEEE Transactions on Image Processing*, 26(7):3142–3155.

Zhang, Y., Zhu, Y., Nichols, E., Wang, Q., Zhang, S., Smith, C., and Howard, S. (2019). A poisson-gaussian denoising dataset with real fluorescence microscopy images. In *Proceedings of the IEEE Conference on Computer Vision and Pattern Recognition*, pages 11710–11718.

A Derivation of Poisson-Gaussian Loss Function

In self-supervised denoising, we only have access to noisy pixels y_i and not the corresponding clean pixels x_i . Similar to a generative model, we use the negative log-likelihood of the training data as our loss function:

$$\mathcal{L}_i = -\log p(y_i) \quad (12)$$

However, for denoising we are interested in learning a model for $p(x_i)$, not $p(y_i)$. We relate $p(x_i)$ to $p(y_i)$ by marginalizing out x_i from the joint distribution:

$$p(y_i) = \int_{-\infty}^{\infty} p(y_i, x_i) dx_i \quad (13)$$

$$= \int_{-\infty}^{\infty} p(y_i|x_i)p(x_i) dx_i \quad (14)$$

In other words, we integrate $p(y_i, x_i) = p(y_i|x_i)p(x_i)$ over all possible values of the clean pixel x_i .

Here, $p(y_i|x_i)$ is simply our chosen noise model. $p(x_i)$ constitutes our prior belief about the value of x_i before we have seen an observation of y_i . We do not know what form the prior should take; it is essentially up to us to choose. Usually we use the conjugate prior of the noise model because this makes the integral tractable.

Our loss function term for pixel i will then be

$$\mathcal{L}_i = -\log \int_{-\infty}^{\infty} p(y_i|x_i)p(x_i)dx_i \quad (15)$$

A.1 Gaussian noise

For zero-centered Gaussian noise, $p(y_i|x_i)$ is the normal distribution centered at x_i with variance equal to σ_n^2 . We choose $p(x_i)$ to be the normal distribution as well. Here we have the network output the parameters of the Gaussian, mean μ_i and std. dev. σ_i .

The marginalized pdf is derived as follows:

$$p(y_i) = \int_{-\infty}^{\infty} p(y_i|x_i)p(x_i)dx_i \quad (16)$$

$$= \int_{-\infty}^{\infty} \frac{1}{\sqrt{2\pi\sigma_n^2}} \exp\left(-\frac{(y_i - x_i)^2}{2\sigma_n^2}\right) \cdot \frac{1}{\sqrt{2\pi\sigma_i^2}} \exp\left(-\frac{(x_i - \mu_i)^2}{2\sigma_i^2}\right) dx_i \quad (17)$$

$$= \frac{1}{\sqrt{2\pi(\sigma_n^2 + \sigma_i^2)}} \exp\left(-\frac{(y_i - \mu_i)^2}{2(\sigma_n^2 + \sigma_i^2)}\right) \quad (18)$$

which we recognize as a Gaussian with mean μ_i and variance $\sigma_i^2 + \sigma_n^2$.

The loss function is then

$$\mathcal{L}_i = -\log p(y_i) \quad (19)$$

$$= -\log\left(\frac{1}{\sqrt{2\pi(\sigma_n^2 + \sigma_i^2)}} \exp\left(-\frac{(y_i - \mu_i)^2}{2(\sigma_n^2 + \sigma_i^2)}\right)\right) \quad (20)$$

$$= \frac{1}{2} \frac{(y_i - \mu_i)^2}{(\sigma_n^2 + \sigma_i^2)} + \frac{1}{2} \log 2\pi + \frac{1}{2} \log(\sigma_n^2 + \sigma_i^2). \quad (21)$$

Dropping the constant terms we have

$$\mathcal{L}_i = \frac{(y_i - \mu_i)^2}{(\sigma_n^2 + \sigma_i^2)} + \log(\sigma_n^2 + \sigma_i^2). \quad (22)$$

A.2 Poisson noise

For high enough values of X_i , the Poisson distribution $\mathcal{P}(\lambda)$ can be approximated by a Gaussian $\mathcal{N}(\lambda, \lambda)$ with mean and variance equal to λ . Using this idea, Laine et al. Laine et al. (2019) adapt the above formulation for Gaussian noise to the Poisson noise case. However, they introduce an approximation in order to evaluate the integral.

Let a be the scaling factor s.t. $y/a \sim \mathcal{P}(x/a)$ where x and y are in the range $[0, 1]$. The noise model using a normal approximation is $y = a(x/a + N(0, x/a)) = x + N(0, ax)$. The proper joint distribution for this model is thus

$$p(y_i)p(x_i) = \frac{1}{\sqrt{2\pi(ax_i)}} \exp\left(-\frac{(y_i - x_i)^2}{2(ax_i)}\right) \cdot \frac{1}{\sqrt{2\pi\sigma_i^2}} \exp\left(-\frac{(x_i - \mu_i)^2}{2\sigma_i^2}\right) \quad (23)$$

However, Laine et al. replace the variance of the noise distribution with $a\mu_i$. This makes the integral tractable. They argue that this approximation is okay if σ_i^2 is small.

$$P(y_i) \approx \int_{-\infty}^{\infty} \frac{1}{\sqrt{2\pi(a\mu_i)}} \exp\left(-\frac{(y_i - x_i)^2}{2(a\mu_i)}\right) \cdot \frac{1}{\sqrt{2\pi\sigma_i^2}} \exp\left(-\frac{(x_i - \mu_i)^2}{2\sigma_i^2}\right) dx_i \quad (24)$$

$$= \frac{1}{\sqrt{2\pi(a\mu_i + \sigma_i^2)}} \cdot \exp\left(-\frac{(y_i - \mu_i)^2}{2(a\mu_i + \sigma_i^2)}\right) \quad (25)$$

which we recognize as a Gaussian with mean μ_i and variance $\sigma_i^2 + a\mu_i$.

Following the derivation above, our loss function is

$$\mathcal{L}_i = \frac{(y_i - \mu_i)^2}{(a\mu_i + \sigma_i^2)} + \log(a\mu_i + \sigma_i^2). \quad (26)$$

A.3 Poisson-Gaussian noise

Noise in microscope images is generally modeled as a Poisson-Gaussian process. The number of photons entering the sensor during the exposure time is assumed to follow a Poisson distribution, and other noise components such as the readout noise and thermal noise are captured by an additive Gaussian term.

We can easily extend the Poisson loss function above to Poisson-Gaussian by adding a noise variance b to the model. Following the derivation above, our loss function is

$$\mathcal{L}_i = \frac{(y_i - \mu_i)^2}{(a\mu_i + b + \sigma_i^2)} + \log(a\mu_i + b + \sigma_i^2). \quad (27)$$

B Posterior mean estimate

The blind-spot network ignores the actual measured value for y_i when it makes a prediction for x_i . However, y_i contains extra information which can be used to improve our estimate of x_i .

Laine et al. Laine et al. (2019) suggest to use the expected value of the posterior:

$$\begin{aligned} \hat{x}_i &= \mathbb{E}[x_i|y_i] = \int_{-\infty}^{\infty} p(x_i|y_i)x_i dx_i \\ &= \frac{1}{Z} \int_{-\infty}^{\infty} p(y_i|x_i)p(x_i)x_i dx_i \end{aligned}$$

where we have applied Baye's rule to relate $p(x_i|y_i)$ and $p(y_i|x_i)p(x_i)$ up to a normalizing constant Z , where

$$Z = \int_{-\infty}^{\infty} p(y_i|x_i)dx_i. \quad (28)$$

For a Gaussian with prior mean μ_i and variance σ_i^2 , and noise variance σ_n^2 , we have the following result:

$$\hat{x}_i = \frac{y_i\sigma_i^2 + \sigma_n^2\mu_i}{\sigma_i^2 + \sigma_n^2} \quad (29)$$

This same formula can be used for the Poisson or Poisson-Gaussian noise models (replacing σ_n^2 with $a\mu_i$ or $a\mu_i + b$, respectively).

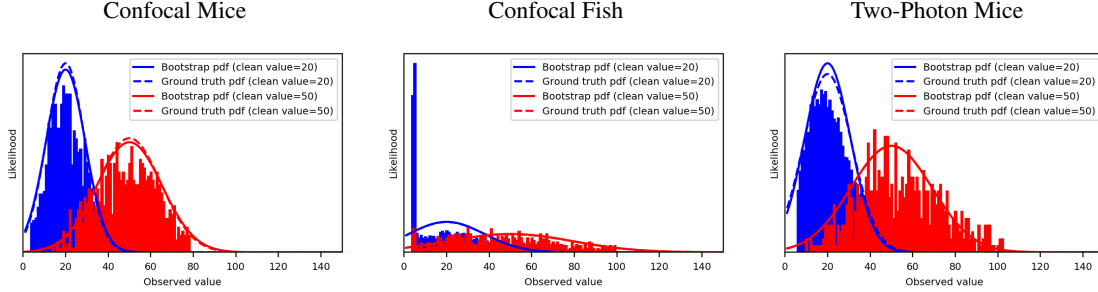


Figure 5: Comparison of Poisson-Gaussian noise models fit to a noisy image from several datasets. The solid bars show histograms of the noisy values corresponding to a clean value of 20 (blue) and 50 (red). The curves show the pdfs of a Poisson-Gaussian distribution fit to the data using either the ground truth clean data (dashed line) or the pseudo-clean data (solid line).

Datasets	Ground Truth Loss	Bootstrap	Ground Truth a	Bootstrap	Ground Truth b	Bootstrap
Confocal Mice	-6.32281348	-6.25717015	0.01813301	0.01964392	-0.00020321	-0.00023262
Confocal Fish	-5.22442770	-5.12222453	0.07531281	0.07230504	-0.00101073	-0.00084717
Two-Photon Mice	-5.00536898	-4.97993000	0.03013427	0.02963781	-0.00055997	-0.00049144

Table 3: Quantitative comparison of fitting a Poisson-Gaussian noise model using the ground truth clean data or the denoised estimate from the prior. Values in the table are averages over the 50 test images from each dataset.

C Extra Results

To evaluate our bootstrapping method, we compare the ground truth and estimated Poisson-Gaussian noise models fit for a test image in each dataset in the FMD benchmark (Zhang et al., 2019). Figure 5 shows that the Poisson-Gaussian pdfs generated using our bootstrapping technique closely match that of the Poisson-Gaussian pdfs generated from the ground truth images.

We further evaluate our approach by comparing the loss and estimated Poisson-Gaussian noise parameters using actual ground truth data or the pseudo-clean data generated in our bootstrap method. Table 3 shows that bootstrapping can provide an accurate estimation of noise parameters and result in a loss similar to that obtained from using ground truth clean data. Here the loss value is

$$\frac{1}{N} \sum_i \left(\frac{(y_i - x_i)^2}{ax_i + b} + \log(ax_i + b) \right) \quad (30)$$

where y_i is a pixel from the noisy image and x_i is a corresponding pixel from either the ground truth clean image or the pseudo-clean image.

Finally, we provide a comparison of denoising results against state-of-the-art fully unsupervised methods. Figure 6 shows zoomed in regions of denoised test images obtained from our method as well as other fully unsupervised methods.

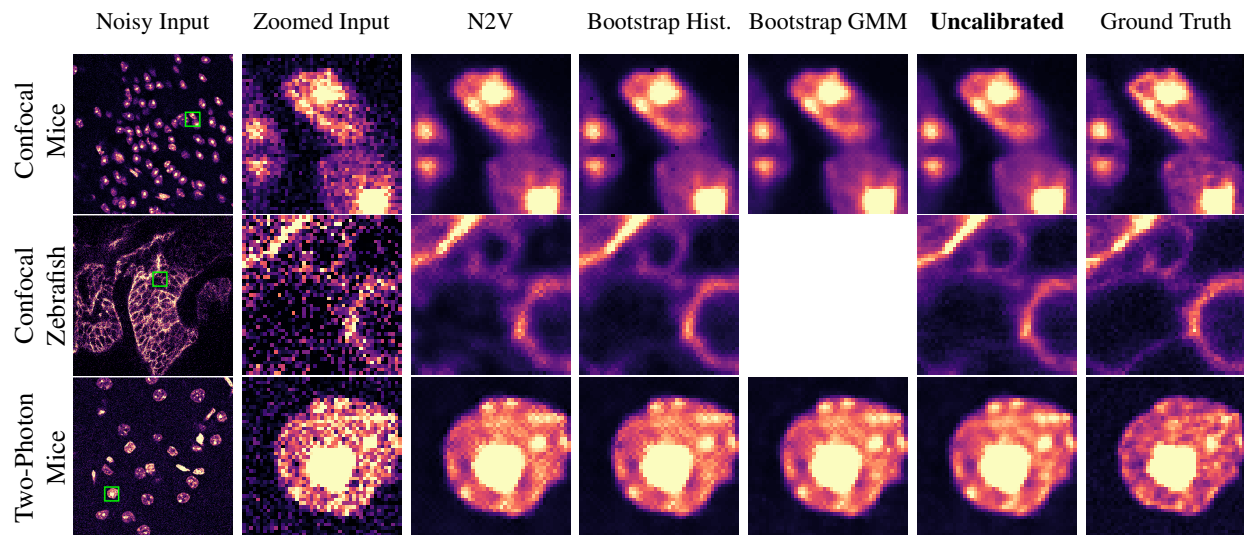


Figure 6: Denoising results on images taken from the FMD dataset (Zhang et al., 2019). Green boxes found in images in the leftmost column denote the regions zoomed in on for qualitative denoising evaluation. The missing image corresponds to the case where the Bootstrap GMM method failed to train.